piece of wood (sample 90-1 in the table) from Mercer's photograph (*27*), we obtained concordant radiocarbon ages from three laboratories of 11,350 ± 90 (AA-9225); 11,240 ± 100 (A-6047); 11,150 ± 160 (Wk-1998); and 11,350 ± 50 years B.P. (Wk-1588); these ages agree with all others in Table 1 and thus we consider them to be accurate. We cannot explain the discrepancies with the dates from Mercer (*27*). Also, Mercer implied that some of the wood was in place. From extensive excavations, we conclude that all the wood pieces in Canavan Knob section were transported.
29. P. Wardle, personal communication.
30. L. R. Basher and M. McSaveney, *R. Soc. N.Z.* **19**, 263 (1989).
31. T. J. H. Chinn, *U.S. Geol. Surv. Prof. Pap. 1386-H*, H25 (1989).
32. J. C. Duplessy, in *Global Changes of the Past*, R. S. Bradley, Ed. (University Center for Atmospheric Research, Office for Interdisciplinary Earth Studies, Denver, CO, 1989), pp. 341–355.
33. S. Björck and P. Möller, *Quat. Res.* **28**, 1 (1987).
34. J. Mangerud, B. G. Andersen, E. Larsen, *Terminat. Pleistocene* **5**, 1 (1992).
35. J. T. Hollin and D. H. Schilling, in *The Last Great Ice Sheets*, G. H. Denton and T. J. Hughes, Eds. (Wiley-Interscience, New York, 1981), pp. 179–206.
36. Funded by the National Science Foundation and the National Geographic Society. C. Schlüchter and H. Conway helped interpret the stratigraphy and radiocarbon samples. We appreciate the cooperation of officials of Westland National Park. We thank R. Kalin and C. Eastoe; A. G. Hogg; and T. M. Jull for radiocarbon analyses. R. N. Patel identified the wood samples. We thank C. Clapperton, G. Jacobson, P. Wardle, R. P. Suggate, S. Björck, T. Chinn, and M. McGlone for helpful comments on the manuscript.

20 December 1993; accepted 25 April 1994

Implications for Mantle Dynamics from the High Melting Temperature of Perovskite

Peter E. van Keken,* David A. Yuen, Arie P. van den Berg

Recent studies have implied that (Mg,Fe)SiO_3-perovskite, a likely dominant mineral phase in the lower mantle, may have a high melting temperature. The implications of these findings for the dynamics of the lower mantle were investigated with the use of numerical convection models. The results showed that low homologous temperatures (0.3 to 0.5) would prevail in the modeled lower mantle, regardless of the effective Rayleigh number and internal heating rates. High-temperature ductile creep is possible under relatively cold conditions. In models with low rates of internal heating, local maxima of viscosity developed in the mid–lower mantle that were similar to those obtained from inversion of geoid, topography, and plate velocities.

Recent experimental results have indicated that the melting temperature of (Mg,Fe)SiO_3-perovskite in the lower mantle may be much higher than earlier estimates suggested (*1, 2*) (Fig. 1). This high melting temperature, increasing from 2500 K at the top of the lower mantle to an extrapolated value of approximately 8000 K at the core-mantle boundary (CMB), would have a profound influence on the flow processes in the lower mantle. We investigated steady-state convection models in order to study the thermal structure and viscosity distribution in the lower mantle with a rheology compatible with the high-temperature melting curve.

For modeling purposes, we linearized the estimates of the melting temperatures from (*1*), according to

$$T_m = 2000 + 2000A_1 z/z_1 \qquad z \geq z_0 \quad (1)$$

where z_1 is the depth of the CMB (3000 km), z_0 is 670 km, and the parameter A_1 is varied between 2 and 3. $A_1 = 3$ gives a melting curve that falls within the range indicated by the three methods of extrapolation (Fig. 1). We set up parameters for the nondimensional viscosity using an Arrhenius type of creep law under Weertman's assumption on the basis of homologous temperature (*3*) as follows:

$$\eta = \exp\left(\frac{A}{T_0 + T}\right)\exp\left(-\frac{A_0}{T_0}\right) \quad (2)$$

where

$$A = \begin{cases} A_0\left[1 + A_1\dfrac{(z - z_0)}{(z_1 - z_0)}\right] & z \geq z_0 \\ A_0 & z < z_0 \end{cases}$$

($z \geq z_0$ refers to the lower mantle; $z < z_0$ refers to the upper mantle). The parameter A can be seen as an activation temperature that increases linearly with depth, following the melting relation (Eq. 1). A_0 is used to scale the maximum viscosity contrast $\Delta\eta$ between the top and bottom of the mantle, which in most cases is taken to be $\Delta\eta = 1000$ (*4*). The temperature T_0 is arbitrarily chosen to be the nondimensionalized lithospheric temperature of 800 K ($T_0 = 0.2$). Varying this parameter will have some consequences for the viscosity distribution in the upper mantle but will not have a strong influence on the viscosity in the lower mantle, which is governed mainly by the increase in melting temperature (Eq. 1) and by the factor A_0 in Eq. 2. The nondimensional equations for momentum and energy are solved for an incompressible Boussinesq fluid at infinite Prandtl number in a two-dimensional Cartesian geometry with an aspect ratio of 1 (*5*). The temperature is scaled to the temperature difference across the layer, on the basis of an estimate of temperature at the CMB of $T_{CMB} = 4000$ K (*6*). The viscosity is scaled to be $\eta = 1$ at the surface.

For a surface Rayleigh number $Ra_s = 10^4$ and viscosity contrast $\Delta\eta = 1000$, we first considered the case where melting temperature is independent of depth (Fig. 2A). The mantle was nearly isoviscous, apart from a viscosity contrast of 1000 across the upper thermal boundary layer. At constant temperature, increasing A_1 gave only a moderate viscosity increase, from a factor of about 20 at $A_1 = 2$ to a factor of 50 at $A_1 = 3$. However, increasing the melting temperature gradient in the lower mantle decreased the internal temperature substantially, and the combined effect increased both the lateral and vertical viscosity contrasts in the lower mantle by several orders of magnitude (Fig. 2, B and C). Deep in the lower mantle, the viscosities varied by four orders of magnitude. A large part of the interior became very cold with increasing A_1, whereas the rising plume was broadened (Fig. 2C). Flow fields were on the order of 10 to 1000 times lower than in the

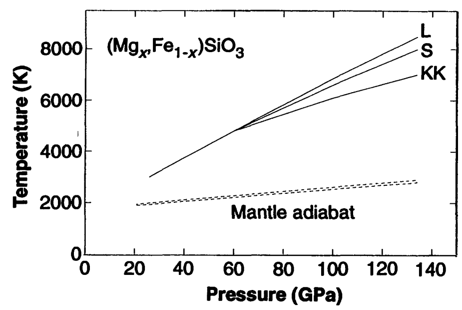

Fig. 1. Melting curve of (Mg,Fe)SiO_3-perovskite, after Zerr and Boehler (*1*). Melting data were obtained between 25 and 62.5 GPa. The solid lines show the fit to the data and extrapolation using Lindemann's law (L) and the Kraut-Kennedy (KK) and Simon (S) melt relations (*1*). The dashed lines indicate a range of estimates for temperatures in an adiabatic mantle (*1*).

P. E. van Keken, Army High Performance Computing Research Center, University of Minnesota, 1100 Washington Avenue South, Minneapolis, MN 55415, USA.
D. A. Yuen, Minnesota Supercomputer Institute, University of Minnesota, 1200 Washington Avenue South, Minneapolis, MN 55415, USA.
A. P. van den Berg, Department of Theoretical Geophysics, Institute of Earth Sciences, Postal Box 80.021, 3508 TA, Utrecht, Netherlands.

*To whom correspondence should be addressed.

upper mantle. This more sluggish lower mantle flow is typical in models with strong depth-dependent viscosity (7). Slow lower mantle flows may account for the relatively fixed position of hot spots over millions of years.

We studied the influence of surface Rayleigh number Ra_s by comparing profiles of horizontally averaged nondimensional temperature $\langle T \rangle$ (8), homologous temperature $\langle T/T_m \rangle$, viscosity $\langle \eta \rangle$, and horizontal velocity u at $x = 0.5$, at $A_1 = 3$, and at $\Delta\eta = 1000$ (Fig. 3A). Interior temperature gradients of $\langle T \rangle$ were only slightly superadiabatic for these purely base-heated ($q = 0$) cases. The thermal boundary layer at the CMB was relatively thick, as compared with that in thermal convection models without depth-dependent activation temperatures. Increasing the Rayleigh number enhanced the efficiency of cooling and produced a very distinct local viscosity maximum in the middle of the lower mantle (9). This formed a style of convection that is reminiscent of penetrative convection, in which the upper mantle circulation drives the sluggish or maybe even passive lower mantle. Because of the high viscosity, at some depths the local Rayleigh number was lower than the critical value (Fig. 3). The models showed an overall moderate convective vigor, as indicated by the Nusselt number Nu (normalized surface heat flux), which varied between 6 (for $Ra_s = 10^3$) and 9 (for $Ra_s = 10^5$) in these models without internal heating.

We further investigated the influences of viscosity contrast $\Delta\eta$ (Fig. 3B) and heating rate q (Fig. 3C). The nondimensional heating rates q = 0, 5, and 9 represented, respectively, a 0, 50, and 90% contribution to the surface heat flow made by internal heating in this situation, and consequently, the Nusselt number increased [$Nu = 15$ for a model with $Ra_s = 10^4$, $\Delta\eta = 1000$, and $A_1 = 3$ (10)]. Larger amounts of internal heating caused the interior temperature to increase strongly, but the homologous temperature in the lowest mantle remained low. The style of lower mantle convection also changed from penetrative convection to a more normal type of cellular convection, because of the reduction of the viscosity maximum and the shift of its position toward the CMB. In some of these Cartesian models, very high internal heating rates created large molten regions in the upper part of the mantle (Fig. 3C), which cannot be considered a realistic feature of the present-day Earth. However, recent calculations with spherical shell geometry indicated that, because of the effect of curvature, the homologous temperature remains low and the viscosity maximum

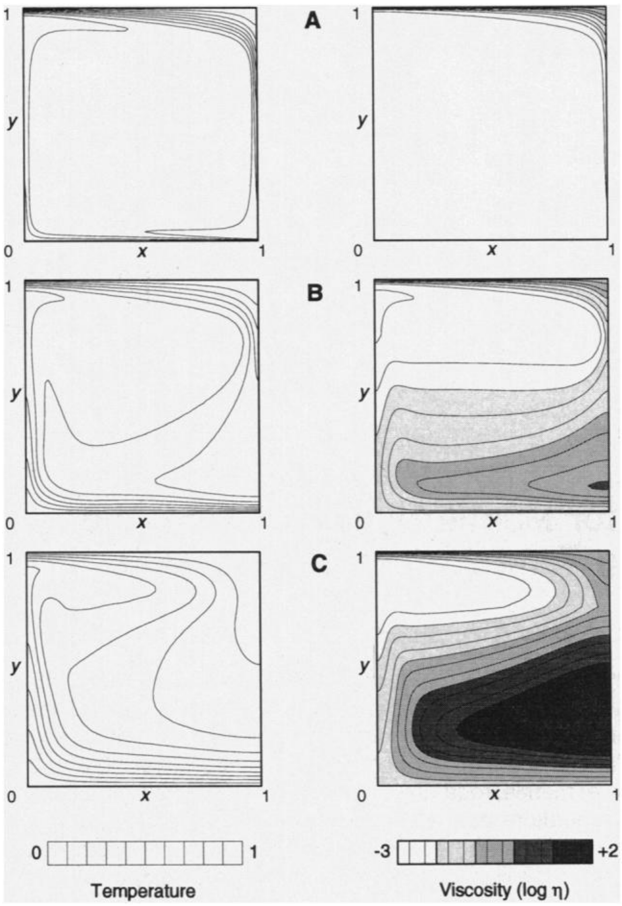

Fig. 2. Steady-state convection results obtained with a viscosity model based on the high melting temperature estimates. The model is heated at the base [temperature is constant at top (T = 0) and bottom (T = 1) of the mantle; no internal heating], and has a surface Rayleigh number of $Ra_s = 10^4$ and viscosity contrast of $\Delta\eta$ = 1000 (3). Shown are nondimensional temperature on the left and viscosity on the right for $A_1 = 0$ (**A**), $A_1 = 2$ (**B**), and $A_1 = 3$ (**C**), where A_1 indicates the gradient of the melting curve (Eq. 1).

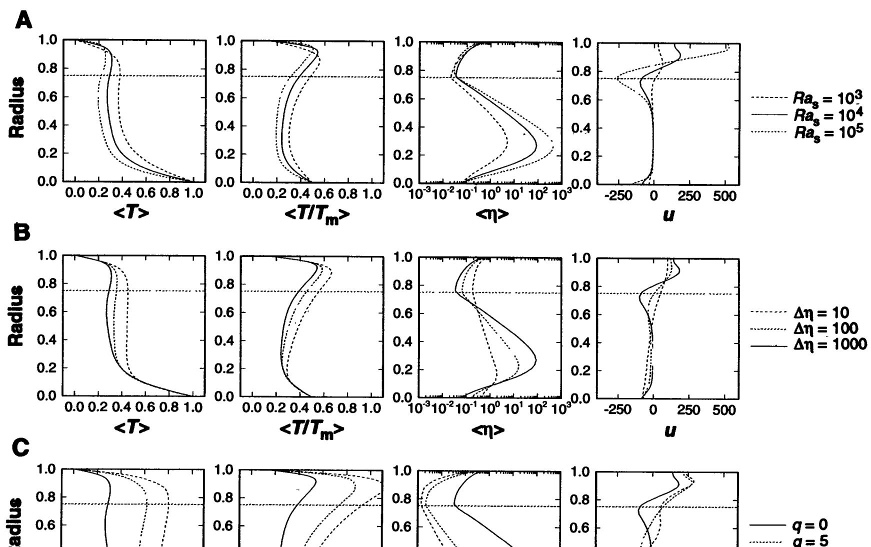

Fig. 3. (**A**) Influence of variation in surface Rayleigh number with depth. Shown are the horizontally averaged nondimensional temperature $\langle T \rangle$, homologous temperature $\langle T/T_m \rangle$, viscosity $\langle \eta \rangle$, and horizontal velocity u at $x = 0.5$, for a purely base-heated model with $\Delta\eta$ = 1000 and $A_1 = 3$. The surface Rayleigh number Ra_s is varied between 10^3 and 10^5. Horizontal dashed line indicates the boundary between upper and lower mantle. (**B**) Influence of variation in viscosity contrast. $Ra_s = 10^4$, $A_1 = 3$, and $\Delta\eta$ is varied between 10 and 1000. (**C**) Influence of rate of internal heating. $Ra_s = 10^4$, $A_1 = 3$, $\Delta\eta = 1000$, and nondimensional internal heating rate q is varied between 0 and 9. This is equivalent to a variation between 0 and 90% internal heating for this model. The solid line indicates the same model ($Ra_s = 10^4$, $\Delta\eta = 1000$, $q = 0$, and $A_1 = 3$) in each of the three rows.

persists, even at high internal heating rates (*11*).

Models developed from inversion of geoid, topography, and plate velocities (*12*) and from postglacial rebound studies (*13*) indicate the presence of a viscosity maximum in the mid–lower mantle. Breaks in seismic spectra are also found at a depth of 1700 km (*14*). Penetrative convection is a well-known phenomenon in fluid mechanics and is particularly associated with the minimum of the thermal expansivity of water at 4°C (*15*). In our models, penetrative convection takes place because of a local viscosity maximum. The idea of penetrative convection in the lower mantle was raised by Peltier (*16*) from linear stability analysis of mantle-like fluids with strong variations in depth-dependent physical properties. This viscosity maximum has also been predicted by asymptotic analysis (*17*). Penetrative convection emerges from the melting temperature estimates of Zerr and Boehler (*1*) in self-consistent, albeit steady-state, calculations in the highly nonlinear regime. The conditions, which are most favorable to the formation of this distinct viscosity maximum and to development of penetrative convection in Cartesian models, are a sufficiently large Ra_s (Fig. 3A), large $\Delta\eta$ (Fig. 3B), and small amounts of internal heating (Fig. 3C).

An important dynamic consequence arising from the melting temperatures of Zerr and Boehler (*1*) is the possible existence of penetrative convection in the lower mantle in situations where internal heating is low. Combined with the estimates for the depth dependence of the coefficient of thermal expansion (*18*) and the thermal diffusivity (*19*), these results would seem to suggest that the lower mantle may play only a minor role in the overall large-scale deformation of the mantle and the surface geophysical signatures, such as the geoid. Recent works (*20*) on geoid anomalies that are based on the time histories of subduction seem to support this view of a passive lower mantle that is subjected to convective forcing from the upper mantle. It is important to corroborate these findings with time-dependent calculations in order to understand better the nature of penetrative convection in the lower mantle that is caused by local viscosity maxima.

REFERENCES AND NOTES

1. A. Zerr and R. Boehler, *Science* **262**, 553 (1993).
2. There has been a recent exchange of different views concerning the two approaches to this difficult laboratory experiment [D. L. Heinz, E. Knittle, J. S. Sweeney, Q. Williams, R. Jeanloz, *ibid.* **264**, 279 (1994); R. Boehler and A. Zerr, *ibid.*, p. 280].
3. J. Weertman and J. R. Weertman, *Annu. Rev. Geophys.* **3**, 293 (1975).
4. We defined $\Delta\eta$ to be the viscosity contrast between top ($T = 0$) and bottom ($T = 1$) of the mantle at constant melting temperature ($A_1 = 0$): for example, $A_0 = 1.658$ for $\Delta\eta = 1000$. The choice of $\Delta\eta$ was not based on laboratory experiments, because of lack of pervoskite creep data, but was instead varied in a range (10 to 1000) that gave reasonable viscosity profiles in the models. Note that in the general case $A_1 \neq 0$, $\Delta\eta$ does not correspond to the viscosity contrast between top and bottom.
5. A. P. van den Berg, P. E. van Keken, D. A. Yuen, *Geophys. J. Int.* **115**, 62 (1993). A finite element method is used to solve the governing equations. We used a penalty function method to solve the equation of motion combined with the incompressibility constraint. Picard iteration was used to obtain steady states efficiently. The geometry was solved with 30 by 30 quadratic, unevenly spaced finite elements. Top and bottom boundaries are constant temperature and stress free. Side boundaries are symmetric.
6. R. Boehler, *Nature* **363**, 534 (1993).
7. L. Fleitout and D. A. Yuen, *J. Geophys. Res.* **89**, 7653 (1984); U. Christensen, *Geophys. J. R. Astron. Soc.* **77**, 343 (1984).
8. The temperature shown here does not include the adiabatic temperature increase. An adiabatic temperature profile would be a vertical line.
9. At $Ra_s = 10^5$, the homologous temperature drops below 0.3, which is considered a lower bound for the high-temperature ductile creep regime for oxides (*3*) [H. J. Frost and M. F. Ashby, *Deformation-Mechanism Maps: The Plasticity and Creep of Metals and Ceramics* (Pergamon, Oxford, 1982)]. For perovskite, no detailed creep data are available. Some care has to be taken in interpreting the results at these low homologous temperatures, because the Weertman type of creep (*3*) used here might not be valid. Under these conditions, low-temperature ductile creep mechanisms are likely to take over from the high-temperature mechanisms.
10. An estimate of the Nusselt number of 10 to 15 is reasonable for the present-day Earth, taking a nominal surface heat flow of 70 mW/m^2 [J. G. Sclater, J. Jaupart, D. Galson, *Rev. Geophys. Space Phys.* **18**, 269 (1980)].
11. P. E. van Keken and D. A. Yuen, *Eos* **75**, 326 (1994).
12. Y. Ricard and B. Wuming, *Geophys. J. Int.* **105**, 561 (1991).
13. E. R. Ivins, C. G. Sammis, C. F. Yoder, *J. Geophys. Res.* **98**, 4579 (1993).
14. W.-J. Su, R. L. Woodward, A. M. Dziewonski, *ibid.* **99**, 6945 (1994).
15. G. Veronis, *Astroph. J.* **137**, 641 (1963); B. Straughan, *Geophys. Astrophys. Fluid Dyn.* **34**, 227 (1985).
16. W. R. Peltier, *Geophys. Fluid Dyn.* **5**, 47 (1973).
17. A. C. Fowler, *J. Geophys.* **53**, 42 (1983).
18. A. Chopelas and R. Boehler, *Geophys. Res. Lett.* **16**, 1347 (1989); *ibid.* **19**, 1983 (1992).
19. M. Osaka and E. Ito, *ibid.* **18**, 239 (1991).
20. S. Zhang and U. R. Christensen, *ibid.* **20**, 2383 (1993); Y. Ricard, M. Richards, C. Lithgow-Bertelloni, Y. LeStunff, *J. Geophys. Res.* **98**, 21895 (1993).

21. P.v.K. is a recipient of an Army High Performance Computing Research Center visiting fellowship grant under contract DAAL03-89-C-0038. This work benefited from discussions with R. Boehler and S. Karato. Supported by a NATO collaboration grant and by the NSF Geochemistry Program.

11 January 1994; accepted 4 April 1994

Species Pool and Dynamics of Marine Paleocommunities

Martin A. Buzas* and Stephen J. Culver

Foraminiferal communities in the Cenozoic shelf deposits of the North American Atlantic Coastal Plain exhibit little unity during almost 55 million years of successive transgressions and regressions. Transgression communities are composed of a dynamic mixture of immigrants and newly evolved species. During regressions, species within these communities either became extinct or emigrated. Some emigrants returned during subsequent transgressions, but many did not. The neritic species of the Atlantic and Gulf continental margins constitute a species pool. Immigrants and emigrants transferred into and out of the species pool, while extinctions and originations repeatedly altered its species composition. While the results indicate a lack of local community unity, at the same time they demonstrate the necessity of a species pool to sustain species diversity.

Some ecological communities have been regarded as a kind of superorganism or unit wherein the component species are closely associated by numerous biotic interactions. Others have been considered as a group of organisms sharing ecological resources in the same time and space but acting independently of one another. Today, most ecologists share a perspective between these two extremes (*1*). Regardless of the initial viewpoint, studies of modern communities encounter difficulties in determining where the component species came from and what becomes of them when their environment ceases to exist.

The fossil record, however, does not have these constraints. The arrival and departure of species, in a given environment, can be documented over millions of years; this record constitutes a ledger, whose entries record the history of a changing community.

During a marine transgression onto a continental shelf, the newly created habitat is quickly occupied by species that are

M. A. Buzas, Department of Paleobiology, National Museum of Natural History, Smithsonian Institution, Washington, DC 20560, USA.
S. J. Culver, Department of Palaeontology, The Natural History Museum, Cromwell Road, London SW7 5BD, UK.

*To whom correspondence should be addressed.